Rezumat

Caracterizarea turbulenței în plasmele de fuziune reprezintă o problemă încă deschisă atât din perspectiva metodelor de diagnoză cât și a celor teoretice. Acest proiect propune contributii la doua aspect importante ale turbulentei : coerenta si efectul deviatiilor de la distributia Gaussiana. Mai precis, prin aceasta lucrare (inclusa in Obiectivul A1) se urmareste sa se determine si sa se inteleaga influenta componentelor cuazi-coerente ale miscarii stohastice si ale potentialului ne-Gaussian asupra transportului turbulent. Se prezinta un studiu detaliat al coerentei Lagrangiene a traiectoriilor in campuri de viteze incompresibile bidimensionale. Proprietatile statistice ale traiectoriilor si ale vitezei Lagrangiene sunt determinate pentru intreg ansamblul R si pentru categoriile de traiectorii capturate si libere, impreuna cu o serie de medii si corelatii conditionate care identifica originea coerentei si efectele asupra transportului. Aratam ca variatia temporala a potentialului nu elimina coerenta Lagrangiana si ca aceasta genereaza memorie de timp lung.
Una dintre proprietățile cunoscute ale câmpurilor turbulente este aceea a caracterului cvasi-Gaussian: distribuția valorilor câmpului este aproape normală. Cu toate acestea, în anumite regiuni și regimuri în cadrul unei descărcări în dispozitive de tip Tokamak, există deviații de la acest caracter. În particular, zona de margine a plasmei, SOL, este caracterizată de fenomene intermitente (ELM, bloburi, unde Alfven) care duc la o deviere puternica de la Gausianitate. În proiectul de față investigăm efectul acestor deviații asupra transportul turbulent al particulelor incarcate. Un model simplu de transport care înglobează driftul ExB și dinamica poloidală este folosit în conjunctură cu o metodă statistică. Efectele sunt estimate analitic și confirmate cu ajutorul simulărilor numerice.

Summary

The characterization of turbulence in fusion plasmas is still an open problem both from the perspective of diagnostic and that of theoretical methods. The project plans to bring contributions in two important aspects of strong turbulence: the coherence and effects of deviation from Gaussian distribution. More precisely, this work (included in the Objective A1) intents to determine and to understand the influence of the quasi-coherent components of the stochastic motion and of the non-Gaussian potential on the turbulent transport. A detailed study of the Lagrangian coherence of the trajectories in 2-dimensional incompressible velocity fields is presented. The statistical properties of the trajectories and of the Lagrangian velocity are determined for the whole ensemble R and for the categories trapped (tr) and free (fr), together with a series of conditional averages and correlations that identify the origin of coherence and the effects on transport. We show that the time variation of the potential does not hinder the Lagrangian coherence and that it generates long time memory.

One of the known properties of the turbulent fields is that of the quasi-Gaussian character: the distribution of field values is almost normal. However, in certain regions and regimes within a discharge in Tokamak-type devices, there are deviations from this character. In particular, the edge region of the plasma, SOL, is characterized by intermittent phenomena (ELM, blobs, Alfven waves) that lead to a strong deviation from Gaussianity. In the current project, we investigate how these deviations affect the turbulent transport of charged particles. A simple transport model incorporating ExB drift and poloidal

dynamics is used in conjunction with a statistical method. The effects are estimated analytically and confirmed with the aid of numerical simulations.

Detailed results

Identification of the hidden coherent components of the turbulent motion. Numerical simulations of intermittency effects on turbulent transport in the SOL and edge plasma.

1. Identification of the hidden coherent components of the turbulent motion.

1.1 Lagrangian coherence

One of the aims of the project is of fundamental nature and is planned to bring a contribution to a main aspect of strong turbulence, the coherence [1]. More precisely this work (included in the Objective A1) intents to determine and to understand the influence of the quasi-coherent components of the stochastic motion (including the recently found hidden drifts [2-4]) on the evolution of turbulence. Quasi-coherence or order appears at the basic level of tracer trajectories in the case of smooth velocity fields that have finite correlation lengths λ and times τ_c. Trajectory coherence (or Lagrangian coherence) is the consequence of the nonlinear equations of motion and it is usually a transitory process with a characteristic time that is limited by the time of flight $\tau_{fl} = \lambda/V$, where V is the amplitude of the stochastic velocity. In two-dimensional incompressible turbulence, coherence can last for much longer time essentially because the trajectories are trapped in the correlated zone.

A detailed study of tracer statistics in 2-dimensional incompressible turbulence was performed at this stage of the project. It is focused on the analysis of the quasi-coherent components of motion. The aim is to identify the hidden order of the motion, to characterize its effect on trajectory statistics and transport and also to understand the nonstandard effects characteristic for two-dimensional incompressible turbulence, which is the basic paradigm in tokamak physics.

The results are based on the numerical simulation of the trajectories and consist on a conditional statistical analysis adapted to the special properties of the two-dimensional incompressible velocity fields. The numerical methods and the original codes [5] have been much developed and already used for several numerical studies of complex transport processes in tokamak plasmas [4], [6].
The results reported here are contained in a paper that is in the process of publication [7].

1.2 The problem and the simulation method

Tracer trajectories in two-dimensional stochastic velocity fields are obtained from

$$\frac{d\mathbf{x}}{dt} = \mathrm{v}(\mathbf{x}, t) = \tilde{\mathrm{v}}(\mathbf{x}, t) + V_d \mathrm{e}_2, \tag{1}$$

where $\boldsymbol{e_1}$, $\boldsymbol{e_2}$ are the unit vectors in the plane of the motion $\boldsymbol{x} = (x_1, x_2)$, $\boldsymbol{e_3}$ is perpendicular on this

plane and the velocity $\boldsymbol{v}(\boldsymbol{x},t)$ has a stochastic component $\tilde{\boldsymbol{v}}(\boldsymbol{x},t)$ superposed on a constant average velocity $V_d = V_d\ \boldsymbol{e}_2$. The incompressibility condition $\nabla \cdot \mathbf{v}(\mathbf{x},t) = 0$ of the velocity field is equivalent with the representation of velocity by a stochastic potential (or stream function) $\varphi(\boldsymbol{x},t)$

$$\tilde{\mathbf{v}}(\mathbf{x},t) = -\nabla\varphi(\mathbf{x},t) \times \mathbf{e}_3. \tag{2}$$

The equation of motion is of Hamiltonian type, with x_1 and x_2 conjugate variables and $\varphi_t(x,t) = \varphi(x,t) + x_1 V_d$ the Hamiltonian function.

Dimensionless quantities are used in Eq. (eqm) with the potential normalized by its amplitude Φ, the distances by λ_0 that is of the order of the correlation lengths, the velocities (including V_d) by $V_0 = \Phi/\lambda_0$ and the time by $\tau_0 = \lambda_0/V_0$.

The potential is represented by a homogeneous and stationary Gaussian stochastic field. Its Eulerian correlation $E(x,t) \equiv \langle \varphi(x_0,t_0)\ \varphi(x_0+x,t_0+t)\rangle$ in dimensionless quantities is modeled in the simulations presented here by

$$E(x,t) \equiv exp\left(-\frac{x_1^2}{2\lambda_1^2} - \frac{x_2^2}{2\lambda_2^2} - \frac{t^2}{2\tau_c^2}\right), \tag{3}$$

where λ_i are the correlation lengths of the 2-dimensional potential and τ_c is the correlation time.

1.3 Main features of tracer advection

The incompressibility of the two-dimensional velocity field determines two invariance laws of the solutions of Eqs. (eqm). It leads to equations of motion of Hamiltonian type, with x_1 and x_2 conjugate variables and φ_t the Hamiltonian function. In the case of time independent (frozen) potentials $\varphi(\boldsymbol{x})$, the trajectories are linked to the contour line of the potential $\varphi_t(x)$, which means that the Lagragian potential $\varphi_t(\boldsymbol{x}(t))$ is invariant along each trajectory. The other invariant law is statistical and applies to the motion in both frozen and time dependent potentials. It concerns the distribution of the Lagrangian velocity $v(\boldsymbol{x}(t),t)$, that is shown to be time independent, and thus identical with the distribution of the Eulerian velocity $v(x,t)$.

The configuration of the contour lines of the potential strongly depend on V_d. At $V_d = 0$ are nested closed curves with multi-scale sizes that have dimensions r_{max} from $r_{max} \ll \lambda_i$ to $r_{max} \to \infty$. The effect of the average velocity is to generate (winding) open paths along its direction by breaking the large size contour lines. Islands of closed contour lines remain between the open paths, but their average size decreases as V_d increases, and, for V_d much larger than the amplitude of the stochastic velocity, all the lines are open. This clearly shows the limitation of the excursion of the contour lines perpendicular to V_d.

This configuration of the contour lines of $\varphi_t(\boldsymbol{x})$ determines solutions of Eq. (eqm) that are, in the presence of an average velocity, a mix of localized periodic (or trapped) trajectories that are closed, and of free trajectories that have unlimited displacements along V_d. The space of trajectories R is organized in two disjointed subensembles: tr for the trapped trajectories and fr for the free ones. The classification criterion is the periodicity of the trajectory. The period T_r of each trajectory is the time of the first return in the initial point $x(0) = 0$, which is determined as the first solution of $r(t) = 0$, where $r(t) = \sqrt{x_1^2(t) + x_2^2(t)}$. The size of each trajectory r_{max} is also calculated. Practically, a trajectory belongs to the subensemble tr when its period is smaller than the time of integration t_{max}.

For $V_d = 0$, all trajectories $x(t)$ are closed, periodic functions of time when $t \to \infty$. At finite time t, open trajectories are found, which correspond to large periods $T > t$ (and to large size contour lines). As t increases the fraction of free trajectories decreases, and, in the limit $t \to \infty$, all trajectories are trapped. The probability of trajectory sizes $P(r_{max}, t)$ is represented in Fig. 1 at two time moments, $t = 60$ (dashed line) and $t = 120$ (solid line). One can see that the time evolution of $P(r_{max})$ affects only the large distances, while the small r_{max} domain has invariant probability. The contributions of the closed and open trajectories to $P(r_{max}, t)$ are also represented in the figure. The closed trajectories (red points) determine the invariant part of $P(r_{max}, t)$. The open trajectories (green points) have large sizes and they determine the time variation of $P(r_{max}, t)$ Their contribution move toward larger r_{max} as time increases and it decays, such that $P(r_{max}, t)$ is determined only by closed trajectories in the limit $t \to \infty$. It is a decaying function of r_{max} that scales as $P(r_{max}, t) \sim r_{max}^{-1.3}$ at large t. The slow algebraic decay of the asymptotic probability shows that the sizes of the trajectories cover multiple scales.

Thus, the invariance of the Lagrangian potential determines a process of trajectory trapping manifested by eddying in the structure of $\varphi(\boldsymbol{x})$.

The average velocity V_d that strongly modifies the structure of the field lines of $\varphi_t(\boldsymbol{x})$ determines a significant change of the probability of trajectory sizes. Two categories of trajectories coexist for $V_d \leq V$: periodic, closed trajectories situated on the islands of closed contour lines of $\varphi_t(\boldsymbol{x})$ and non-periodic trajectories along the open paths generated by the average potential xV_d. The latter are free trajectories that make large displacements along V_d. The probability $P(r_{max}, t)$ can be written as the sum of the contributions of these two types of trajectories

$$P(r_{max}, t) = n_{tr}(r_{max}, t) + n_{fr}(r_{max}, t) \tag{5}$$

where n_{tr}, n_{fr} are determined in the subensembles tr and fr at time t. $P(r_{max}, t)$ shown in Fig. 2 (left panel) has a second maximum. It appears at a large value of r_{max} that increases with the increase of V_d. Also, the amplitude and the width of this peak increase with V_d and eventually saturate. It is determined by the free trajectories. The narrow peak at small r_{max} is the contribution of the trapped, periodic trajectories $n_{tr}(r_{max}, t)$. It is represented in the right panel of Fig. 2, which shows that both the maximum size and the amplitude of the trapped trajectories decrease as V_d increases. The average velocity hinders and eventually eliminates the trapping process. The contribution $n_{tr}(r_{max}, t)$ in Eq. (5) decreases with V_d and become negligible at $V_d \gg 1$. The contribution of the free trajectories is negligible in this range of small sizes, at any V_d, as shown in Fig.2 (right panel) where the black points for $P(r_{max}, t)$ are superposed on the red curves for $n_{tr}(r_{max}, t)$.

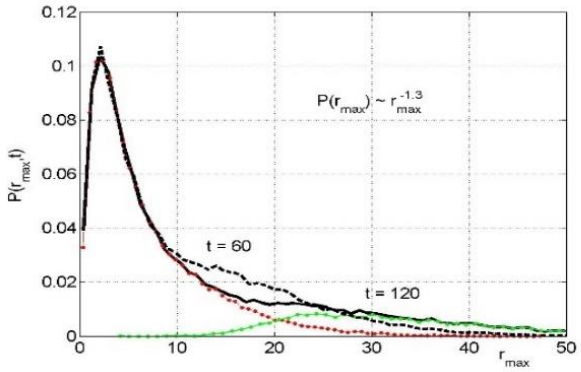

FIG. 1: The probability of trajectory sizes P(rmax, t) for Vd = 0 at t = 60 (dashed black line) and t = 120 (solid black line). Also shown are the contributions of the trapped (red points) and free (green points) trajectories at t = 120.

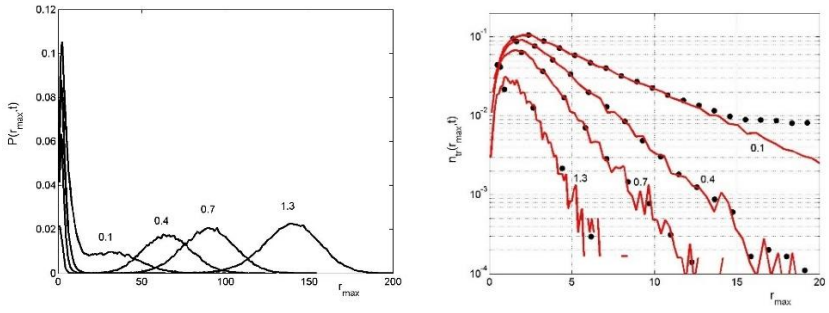

FIG. 2: The probability P(rmax, t) for several average velocities Vd that label the curves, at t = 60 as function of rmax (the curves in the left panel and black points in the right panel) and the contribution of the trapped trajectories ntr(rmax, t) (right panel, red lines).

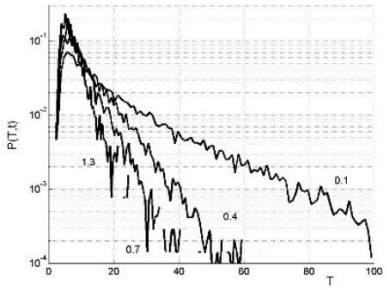

FIG. 3: The probability of the periods of the trapped trajectories P(T, t) as functions of T at t = 60 and at the values of Vd that label the curves.

The probability of the periods of the closed trajectories $P(T,t)$ calculated from the trajectories $\boldsymbol{x}(t)$ at $t = 60$ is shown in Fig. 3. One can see that, at small V_d, this probability extends to large values of $T{\sim}100$ and it has an weak decay. As V_d increases, the width of $P(T,t)$ decreases and its decay is steeper (in agreement with the decay of the trajectory sizes at large V_d).

The fraction of trajectories that are not closed at time t, $n_{fr}(t,V_d)$ is obtained from the probability of the periods of the closed trajectories (calculated at the time of integration, t_{max})

$$n_{fr}(t,V_d) = 1 - \int_0^t P(T,t_{max})\, dT. \tag{6}$$

This function decreases in time from $n_{fr}(0,V_d) = 1$, as seen in Fig. 4 (left panel). In the case $V_d \neq 0$, $n_{fr}(t,V_d)$ saturates at a value $n_{fr}(V_d)$ in a time that becomes shorter at larger V_d . In the case of $V_d = 0$, the decay is not limited, and it scales as $n_{fr}(t,0) \sim t^{-0.6}$.

The results obtained for the asymptotic fraction of free trajectories $n_{fr}(V_d) \equiv \lim_{t\to\infty} n_{fr}(t,V_d)$, presented in Fig. 4 (right panel), are well approximated by

$$n_{fr}(V_d) = \left[1 - exp\left(-V_d^2\right)\right]^{1/4}. \quad (7)$$

The fraction of trapped trajectories is $n_{tr}(t, V_d) = 1 - n_{fr}(t, V_d)$ at any time, with the asymptotic value $n_{tr}(V_d) = 1 - n_{fr}(V_d)$ that is also represented in Fig. 4 (right panel).

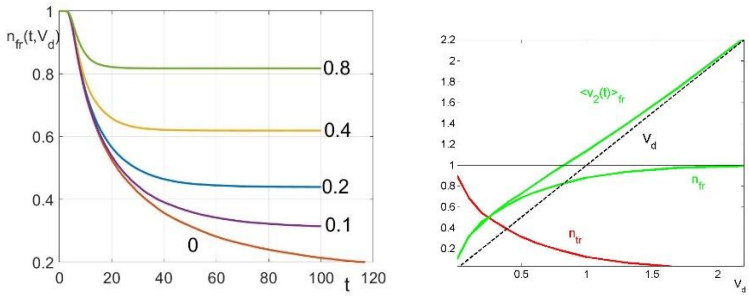

FIG. 4: Left panel: the fractions of free trajectories as function of time for the values of V_d that label the curves. Right panel: the asymptotic values n_{fr} and n_{tr} and the average velocity of the free trajectories as functions of Vd.

Thus, the trajectories obtained in the stochastic potential $\varphi_t(\boldsymbol{x})$ were divided into two categories: trapped and free. They have different topologies and different sizes, which suggests that their contributions to the global statistical properties of the trajectories are qualitatively different.

We analyze in the next two sections the statistics of the Lagrangian velocity and of the displacements of each category of trajectories. For any Lagrangian quantity $A(\boldsymbol{x}(t))$, we determine $\langle A(\boldsymbol{x}(t))\rangle_{tr}$ and $\langle A(\boldsymbol{x}(t))\rangle_{fr}$ that are conditional averages restricted to the trapped and free trajectories, respectively. These are statistical averages calculated over the subspaces tr and fr. The contribution of each subensemble to the global average (over R) is the product of the probability that a trajectory belongs to the subensemble multiplied by the statistical average over the subensemble, $n_c\langle A(\boldsymbol{x}(t))\rangle_c$, where $c = tr,\ fr$. It yields

$$\langle A(\boldsymbol{x}(t))\rangle = n_{tr}\langle A(\boldsymbol{x}(t))\rangle_{tr} + n_{fr}\langle A(\boldsymbol{x}(t))\rangle_{fr}. \quad (8)$$

The separation of the trajectories in these categories is performed at a large time such that $n_{fr}(t, V_d)$ is saturated (see Fig. 4, left panel).

1.4 Statistics of the Lagrangian velocity

The statistical parameters of the Lagrangian velocity $v(\boldsymbol{x}(t)) \equiv v(t)$ are shown in Fig. 5 for a stochastic potential with $\lambda_1 = 1,\ \lambda_2 = 2$ and $V_d = 0.2$. The average Eulerian velocity and fluctuation amplitudes are in this case $\langle v_1\rangle = 0,\ \langle v_2\rangle = V_d,\ V_1 = 0.5$ and $V_2 = 1$.

The Lagrangian quantities maintain the Eulerian values at any time, as stated by Lumley theorem. Besides this, the conditional average velocity and fluctuation amplitudes are time invariant, as seen in Fig. 5, but they have values significantly dependent on the category.

It is interesting to note that the average velocity is determined only by the free trajectories, while the trapped trajectories do not contribute ($\langle v_2(t)\rangle_{tr} = 0$ at any time). The average velocity of the free

trajectories is larger that V_d, and it can be approximated with

$$\langle v_2(t)\rangle_{fr} = \frac{V_d}{n_{fr}} > V_d \tag{9}$$

It is $\langle v_2(t)\rangle_{fr} = 0.45$ for the example presented in Fig. 5, left panel, obtained for $V_d = 0.2$. The conditional average velocity $\langle v_2(t)\rangle_{fr}$ is also shown in Fig. 4 (right panel) as function of V_d. One can see that this average velocity is significantly larger than V_d only in the presence of trajectory trapping (for $V_d < 1$). A supplementary ordered component of the Lagrangian velocity appears for the free trajectories that exactly compensates the missing contribution of the trapped particles, such that $\langle v_2(t)\rangle = n_{fr}\langle v_2(t)\rangle_{fr} = V_d$. This result seems to be a trivial consequence of $\langle v_2(t)\rangle_{tr} = 0$, but the underlying physical process is rather complex. It essentially consists of generation of ordered motion from the stochastic velocity for both types of trajectories

$$\langle \tilde{v}_2(t)\rangle_{tr} = -V_d,\ \langle \tilde{v}_2(t)\rangle_{fr} = V_d \frac{n_{tr}}{n_{fr}} \tag{10}$$

The supplementary average velocity of the trapped trajectories is opposite to $\boldsymbol{V}_d$ and exactly compensates it. The supplementary average velocity of the free trajectories is along $\boldsymbol{V}_d$ and it contributes to the increase of the Lagrangian over the Eulerian velocity.

Equations (10) are valid at any time, including $t = 0$. It can be interpreted as the condition for the separation of the trajectories in the free and trapped categories. The trapped trajectories start from the geometric locus for which $\langle \tilde{v}_2(\boldsymbol{x})\rangle_{tr} = -V_d$ and they remain in this domain, while the free trajectories are confined in the complement of this domain. These ordered components of the motion are hidden, in the sense that they are not "seen" in the average velocity calculated on the whole ensemble R ($\langle v_2(t)\rangle = V_d$). However, as shown below, they have strong effects on the transport along V_d through the modification of the correlation of the Lagrangian velocity.

The amplitudes of velocity fluctuations around the average velocity are shown in Fig. 5 (right panel). They are different for the two types of trajectories. It is interesting to underline that the supplementary order that characterizes trapped and free trajectories appears in the fluctuations of the velocity in R. The average of the square velocity decomposed on tr and fr subensembles according to Eq. (8)

$$\langle v_i^2(t)\rangle = n_{tr}\langle v_i^2(t)\rangle_{tr} + n_{fr}\langle v_i^2(t)\rangle_{fr}, \tag{11}$$

leads to

$$V_2^2 = n_{tr}(V_2^{tr})^2 + n_{fr}(V_2^{fr})^2 + \frac{n_{tr}}{n_{fr}}V_d^2, \tag{12}$$

$$(V_i^c)^2 \equiv \langle (v_i(t) - \langle v_i(t)\rangle_c)^2\rangle_c \tag{13}$$

are the amplitudes of the fluctuations of the velocity $\delta v_i(t) \equiv v_i(t) - \langle v_i(t)\rangle_c$, $i = 1,2$, conditioned by the category of trajectories $c = tr,\ fr$ (on the subensembles tr and fr). Thus, a contribution produced by the ordered motion appears (the last term of Eq. (12) besides the direct contributions of the conditional fluctuations. It is determined by ordered motion (10) generated by V_d in the presence of trapping (for $0 < V_d < 1$). The results presented in Fig. 5 (right panel) show values $V_2^{tr} < V_2$ and $V_2^{fr} < V_2$, which reproduce Eq. (12).

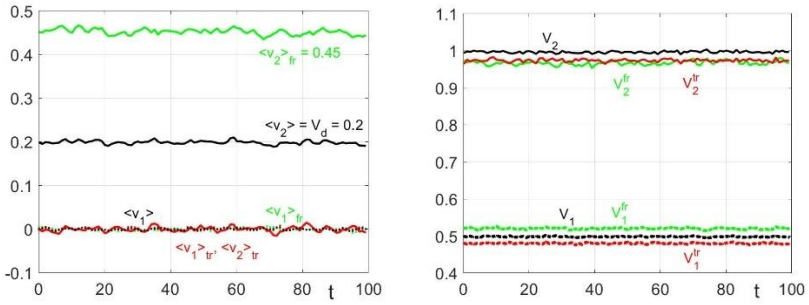

FIG. 5: The average Lagrangian velocities (left) and the fluctuations of the Lagrangian velocities (right) as functions of time. The dashed lines are for v_1 and the solid lines for v_2. Green is for the free and red for trapped trajectories, while black are averages on the whole statistical ensemble R. $V_d = 0.2$.

The conditioned amplitudes of the velocity fluctuations V_i^c depend on the average velocity V_d. As seen in Fig. 6, the amplitudes of both components of the trapped trajectory velocity (red curves) are continuously decreasing functions of V_d . This is the effect of the decrease of the size of the islands of closed contour lines of the potential, which, as V_d increases, shrink around the maxima and minima of $\varphi(x)$ where the gradients are small. In the case of free trajectories (green lines), the amplitudes of the Lagrangian velocities are different of V_i only in the range of V_d that corresponds to the existence of islands of closed contour lines of the potential. The perpendicular amplitude is increased ($V_1^{fr} > V_1$), while the parallel amplitude is decreased ($V_2^{fr} < V_2$) such that the supplementary parallel velocity is compensated (Eq. 12).

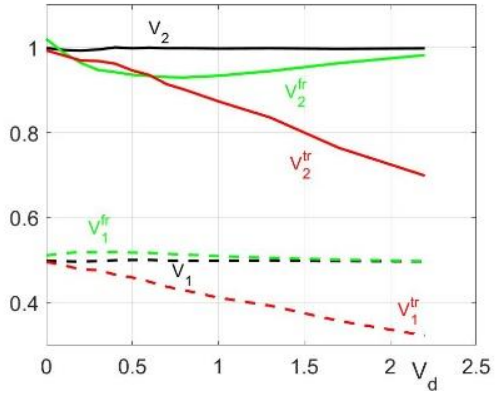

FIG. 6: The amplitudes of fluctuations of the Lagrangian velocities as functions of Vd. The dashed lines are for v_1 and the solid lines for v_2. Green is for the free and red for trapped trajectories, while black are averages on the whole statistical ensemble R.

One can deduce from these results that the EC defined on the geometric locus of the free trajectories is different of the EC (3). The amplitude of the stochastic potential is smaller ($\Delta < \Phi$) and the correlation lengths are modified.

$$\lambda_1^{fr} = \lambda_1 \frac{\Delta}{\Phi} \frac{V_2}{V_2^{fr}}, \ \lambda_2^{fr} = \lambda_2 \frac{\Delta}{\Phi} \frac{V_1}{V_1^{fr}}, \tag{14}$$

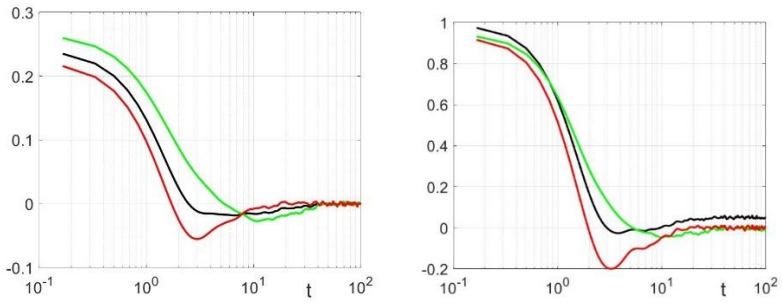

FIG. 7: The correlations of the Lagrangian velocity $v_1(t)$ (left) and $v_2(t)$ (right) calculated on the whole statistical ensemble $L_i(t)$ (black lines) are compared to the conditioned correlations $L_i^{tr}(t)$ (red lines) and $L_i^{fr}(t)$ (green lines). $V_d = 0.2$.

The correlations of the Lagrangian velocity are shown in Fig. 7, where the notations are

$$L_i(t) = \langle \delta v_i(0)\ \delta v_i(t) \rangle,\ L_i^c(t) = \langle \delta v_i(0)\ \delta v_i(t) \rangle_c. \tag{15}$$

One can see that all the conditional correlations (for both categories and both components of the velocity) decay to zero at large t. However, the correlation of the velocity along V_d calculated on all trajectories, $L_2(t)$, has a finite asymptotic value. It is determined by the ordered components of motion produced in subensembles tr and fr. An equation similar to (12) can be obtained from (8) written for $A = v_i(0)\ v_i(t)$

$$L_2(t) = n_{tr} L_2^{tr}(t) + n_{fr} L_2^{fr}(t) + \frac{n_{tr}}{n_{fr}} V_d^2, \tag{16}$$

which shows that $L_2(t)$ has a finite asymptotic tail in spite of the decay to zero of $L_2^{tr}(t)$ and $L_2^{fr}(t)$. It is determined by the presence of trapped trajectories at small average velocity V_d.

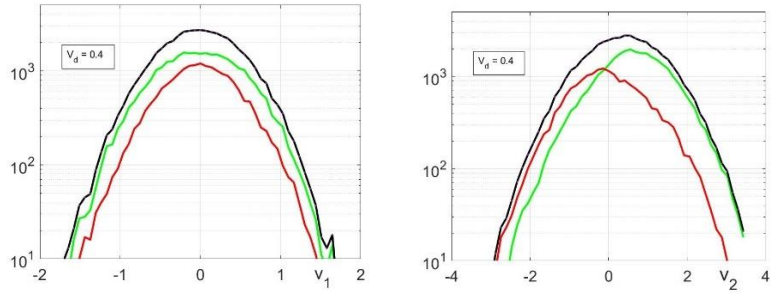

FIG. 8: Histograms of the Lagrangian velocities v_1 (left) and v_2 (right) represented by black curves and the contributions from the free (green curves) and trapped (red curves) trajectories.

The histograms for the Lagrangian velocity components are time invariant for all statistical ensembles R, tr and fr. The histogram for all trajectories (in R) is shown in Fig. 8 together with the contributions of the trapped and free trajectories. One can see that the distribution is Gaussian in R, while significant departures from Gaussianity appear in the subensembles tr and fr, especially for the velocity component v_2 (right panel).

1.5 Statistics of trajectories

The statistics of the displacements is strongly non-Gaussian, in spite of the Gaussian Lagrangian velocity. Moreover, it is not invariant, but characterized by a transitory initial regime with variation of the time dependence. Asymptotic regimes with well defined time-dependence are reached for the average and mean square displacements (calculated for all trajectories and in the subensembles tr and fr). As discussed below, these regimes can be linear, quadratic or saturated.

The average displacements are in agreement with the average Lagrangian velocities

$$\langle x_1(t)\rangle = \langle x_1(t)\rangle_{tr} = \langle x_1(t)\rangle_{fr} = 0, \qquad (17)$$
$$\langle x_2(t)\rangle = V_d t,\ \langle x_2(t)\rangle_{tr} = 0,\ \langle x_2(t)\rangle_{fr} = \frac{V_d}{n_{fr}} t.$$

The dispersion $\langle(\delta x_i(t))^2\rangle$, where $\delta x_i(t) = x_i(t) - \langle x_i(t)\rangle$ are shown in Fig. 9 for $V_d = 0$ (left panel) and for $V_d = 0.2$ (right panel), compared to the results obtained for the trapped $\langle(\delta x_i(t))^2\rangle_{tr}$ and free $\langle(\delta x_i(t))^2\rangle_{fr}$ trajectories. One can see that the dispersions of the trapped trajectories (the red curves in Fig. 9) saturate in both cases, for both directions, $\langle(\delta x_i(t))^2\rangle_{tr} \to const$. This means that the trapped trajectories do not contribute to the transport in static potential.

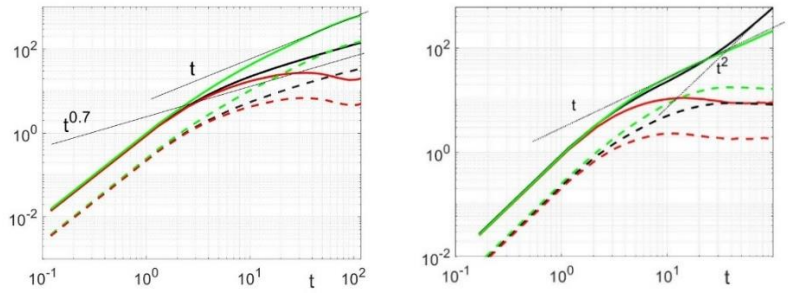

FIG. 9: The dispersions of the trajectories for $V_d = 0$ (left) and $V_d = 0.2$ (right) (black lines) compared to the dispersions for trapped (red) and free (green) trajectories. The dashed lines are for $x_1(t)$ and the solid lines for $x_2(t)$.

In the absence of the average velocity ($V_d = 0$), the dispersions are similar along the two directions. The curves in the left panel of Fig. 9 are only translated due to the different amplitudes of the stochastic velocities $V_1 = 0.5$, $V_2 = 1$. The free trajectories have a normal diffusive evolution $\langle(\delta x_i(t))^2\rangle_{fr} \sim t$ in both directions, while the dispersion of all trajectories is sub-diffusive with time increase that is slower than linear $\langle(\delta x_i(t))^2\rangle \sim t^{0.7}$. This is the result of the time dependence of the fraction of free trajectories $n_{fr}(t, V_d)$, which is a decreasing function of time (see Fig. 4, left panel).

The average velocity V_d makes trajectory dispersion strongly non-isotropic. The dispersions across V_d (of $x_1(t)$) for the whole set of trajectories and for the subensembles tr and fr are all saturated (the dashed curves in Fig. x2, right panel). This means that the average velocity completely hinders the transport perpendicular to its direction in the case of static stochastic potentials. The contrary happens to the transport parallel to V_d: the dispersion of the trajectories has a very fast time-increase, $\langle(\delta x_2(t))^2\rangle \sim t^2$, which correspond to the maximum super-diffusive transport that is of the ballistic type. It appears in spite of the much weaker transport of the trapped and free trajectories ($\langle(\delta x_2(t))^2\rangle_{tr}$

saturates and $\langle(\delta x_2(t))^2\rangle_{fr} \sim t$ is diffusive).

This super-diffusive transport along the average velocity can be demonstrated using Eq. (8) for $A = x_i^2(t)$. The relations between the dispersion of all trajectories (in R) and the subensemble tr and fr dispersions are

$$\langle(\delta x_1(t))^2\rangle = n_{tr}\langle(\delta x_1(t))^2\rangle_{tr} + n_{fr}\langle(\delta x_1(t))^2\rangle_{fr}, \tag{18}$$

$$\langle(\delta x_2(t))^2\rangle = n_{tr}\langle(\delta x_2(t))^2\rangle_{tr} + n_{fr}\langle(\delta x_2(t))^2\rangle_{fr} + \frac{n_{tr}}{n_{fr}} V_d^2\ t^2. \tag{19}$$

The last term in Eq. (19) is dominant at large time and it makes the asymptotic regime superdiffusive of ballistic type. This term is determined by the supplementary average velocity generated from the stochastic components for the free and trapped trajectories, Eq. (10). It leads to the 'concentration' of the average velocity along the free trajectories. The super-diffusive transport is determined by the average velocity ($V_d \neq 0$) only in the presence of the islands of trapped trajectories ($n_{tr} \neq 0$), which corresponds to $V_d < 1$.

The probability of the displacements (Fig. (10)) is strongly non-Gaussian due to the trapped trajectories that have a peaked distributions around the starting point x=0. The free trajectories have Gaussian distribution in both directions with the average velocity (9) along $\boldsymbol{V}_d$ that is significantly greater than V_d.

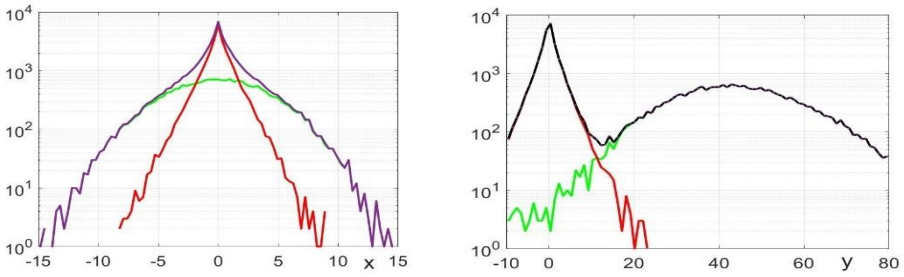

FIG. 10: The histogram of $x_1(t)$ (left) and $x_2(t)$ (right) for the whole set of realizations (black) compared to the contributions of the free (green) and trapped (red) trajectories at t=97. $V_d = 0.2$.

1.6 Coherence induced by an average velocity

The Hamiltonian structure of equation (1) is the origin of the order that characterizes the two-dimensional incompressible turbulence. It determines the strong connection between trajectories and the contour lines of the potential, which are paths of the motion. The order (quasi-coherence) of the motion is essentially represented by the existence of correlations between the potential and the trajectories. They are represented by nonzero average displacements or velocities conditioned by the (initial) potential.

Significant quasi-coherent characteristics of the transport process can be found by analyzing statistical Lagrangian quantities restricted on the contour lines with given potential φ^0. The trajectories that belong to this class correspond to solutions of Eq. (1) that start (in $x(0) = 0$) from points with $\varphi(0) = \varphi^0$. The invariance of the total potential in this class gives

$$\varphi_t(x(t)) = \varphi(x(t)) + x_1(t)V_d = \varphi^0. \tag{20}$$

The fractions of trajectories that evolve on the φ^0 potential lines, the average and the amplitude of fluctuations of their displacements and Lagrangian velocities are determined below for each type of trajectories using conditional averages.

The analysis starts from the representation (8) and introduces a supplementary condition for the trajectories, namely that the initial potential is φ^0 $[\varphi(x(0)) = \varphi^0]$. We have obtained an equation that links the average conditioned by φ^0 to the averages restricted to each category tr or fr

$$\langle A(x(t))\rangle_{\varphi^0} P(\varphi^0) = \langle A(x(t))\rangle_{\varphi^0,tr} n^{tr}(\varphi^0) + \langle A(x(t))\rangle_{\varphi^0,fr} n^{fr}(\varphi^0). \quad (21)$$

In particular, for $A = 1$, the fractions of trajectories for each category fulfil the equation

$$P(\varphi^0) = n^{tr}(\varphi^0) + n^{fr}(\varphi^0). \quad (23)$$

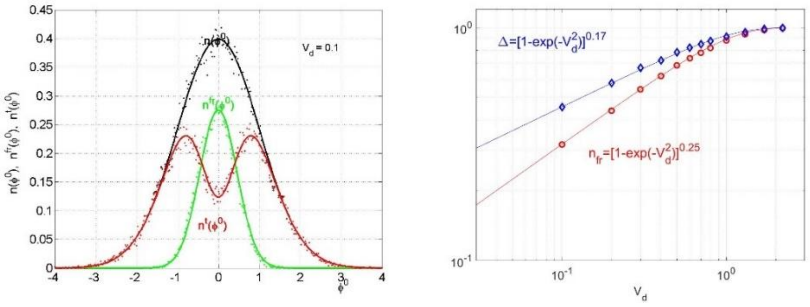

FIG 11: Left panel: The fraction of the trajectories that evolve on the contour lines with potential φ^0 for the free (green points), trapped (red points) and for all trajectories (black points) compared to $P(\varphi^0)$ (black line), with Eq. (24) (green line) and Eq. (23) (red line). Right panel: The width Δ of the initial potential of the free trajectories (diamonds) and the fraction of free trajectories (circles) as functions of the average velocity V_d.

The numerical results obtained for $n^{fr}(\varphi^0)$ and $n^{tr}(\varphi^0)$ (represented by points), are compared to analytical approximations (solid lines) in Fig. 11 (left panel). We have found a good approximation of the data by

$$n^{fr}(\varphi^0) = n_{fr}\ G(\varphi^0; \Delta), \quad (24)$$

where $G(\varphi^0; \Delta)$ is the Gaussian distribution

$$G(\varphi^0; \Delta) = \frac{1}{\sqrt{2\pi}\Delta} exp\left(-\frac{(\varphi^0)^2}{2\Delta^2}\right) \quad (25)$$

with a width Δ that depends on the average velocity V_d. The fraction of the trapped trajectories obtained from Eq. (23) (red curve) provides a good representation of the numerical results.

The width Δ as function of the average velocity V_d is shown in Fig. 11 (right panel) together with the fraction of free trajectories n_{fr}. Both functions saturate at large V_d, and they have power law dependence for small V_d

$$n_{fr} \sim V_d^{0.5},\ \Delta \sim V_d^{0.34}, \tag{26}$$

$$\Delta(V_d) = \left[1 - exp\left(-V_d^2\right)\right]^{0.17}. \tag{27}$$

Thus, most of the free trajectories are localized on the contour lines with small values of $|\varphi^0| \leq \Delta$. The trapped (periodic) trajectories mainly have large $|\varphi^0|$: they completely occupy the range of large potential $|\varphi^0| \gg \Delta$, but have significant presence in the range of the free trajectories.

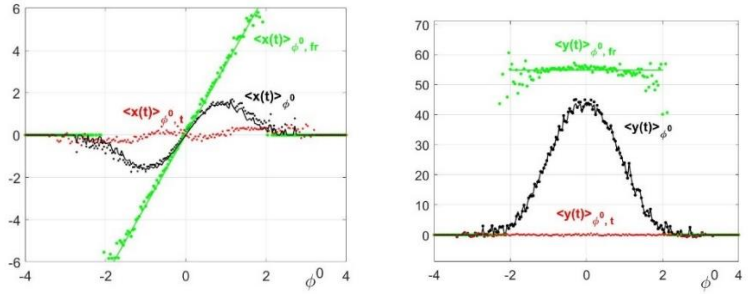

FIG. 12: The conditional average as functions of φ^0 for the trapped (red), free (green) and all (black) trajectories, compared to the approximations (28). $V_d = 0.3$.

The average displacements conditioned by the value of the initial potential and by the category of the trajectories are shown in Fig. 12 at $t = 97$, larger than the saturation time of $n_{fr}(t, V_d)$. These represent quasi-coherent components of the motion, and appear only in the presence of an average velocity. One can see that the average conditional displacements are small for the trapped trajectories (red points), and that significant values appear for the free trajectories in both directions (green points). As shown in Fig. 12, these quantities can be approximated by

$$\langle x_1(t)\rangle_{\varphi^0,fr} = \frac{\varphi^0}{V_d},\ \ \langle x_1(t)\rangle_{\varphi^0,tr} \cong 0,\ \ \langle x_2(t)\rangle_{\varphi^0,fr} = \frac{V_d t}{n_{fr}},\ \ \langle x_2(t)\rangle_{\varphi^0,tr} = 0, \tag{28}$$

which are represented by red and green lines respectively. The black lines have the equations

$$\langle x_1(t)\rangle_{\varphi^0} = \frac{\varphi^0}{V_d} F(\varphi^0),\ \ \langle x_2(t)\rangle_{\varphi^0} = \frac{V_d t}{n_{fr}} F(\varphi^0),\ F(\varphi^0) = \frac{n^{fr}(\varphi^0)}{P(\varphi^0)} = \frac{n_{fr}}{\Delta} exp\left(-\frac{(\varphi^0)^2}{2}\frac{1-\Delta^2}{\Delta^2}\right). \tag{29}$$

The parallel average displacement on the contour lines with initial potential φ^0, leads to an average Lagrangian velocity that does not depend on φ^0 and equals the average velocity of the free trajectories (9).

1.7 Time dependent potentials

The general conclusion of the analysis of trajectory statistics in frozen potentials is the existence of a high degree of coherence, which reflects the structure of the contour lines of $\varphi(\boldsymbol{x})$ on which the trajectories are bounded. The time-dependence of the potential determines the variation of the Lagrangian potential and the decorrelation from its initial value φ^0. It is expected to strengthen the random aspects of the trajectories and to cause the elimination of the Lagrangian coherence in a time of the order of the decorrelation time τ_c. It is thus expected that the order found in static potential is in this case only a transitory processes with life-time τ_c.

The trajectories are more complex than in static potentials. Closed periodic trajectories do not exist in time dependent potentials, but trapping events represented by almost closed eddying segments appear on all trajectories when the decorrelation time τ_c is large compared to the time of flight $\tau_{fl} = \lambda/V$ and the integration time is much longer than τ_c. The trapping events are separated by long jumps, which are similar with the free trajectories. The trajectories are not linked on the lines (20) that represent the invariance of the total Lagrangian potential in the space $\varphi\big(\boldsymbol{x}(t)\big) - x_1(t)$, but they diffuse to neighbour lines around the initial potential.

The separation of the trajectories in the categories $c = tr,\ fr$ has no meaning in time-dependent potentials. However one can define related quantities that are not properties of the trajectories but of the contour lines of the potential. The latter are geometric objects. The fraction of free/trapped trajectories can be defined using the number of trajectories that stay on open/closed contour lines of the potential at time t. These fractions do not depend on time for stationary stochastic potentials, because the amplitude, the space correlation and the structure of the contour lines are statistically time-invariant. They equal the asymptotic values of $n_c(t, V_d)$ obtained in static potentials from the trajectories

$$n_c(V_d) = \lim_{t\to\infty} n_c(t, V_d), \tag{30}$$

for any τ_c and $c = tr, fr$. In a similar way, the fraction of trajectories that stay at time t on a contour lines of category c with the potential $\varphi^t = \varphi(\boldsymbol{x}(t))$ is a time-independent function of φ^t and c, which is the asimptotic value $n^c(\varphi^t)$ of the fractions obtained in static potential ($\tau_c \to \infty$) in Eqs. (24).

- Hidden ordered motion

Ordered motion conditioned by the initial potential φ^0 was found in the presence of an average velocity V_d for the free trajectories. It is represented by the average displacements $\langle x_i(t)\rangle_{\varphi^0, fr}$ that are conditioned by the initial potential and by the category $c = fr$ [Eq. (28)]. These quantities obtained in a time-dependent potential (with $\tau_c = 33$) are shown in Fig. (13) for x_1, compared to the static case.

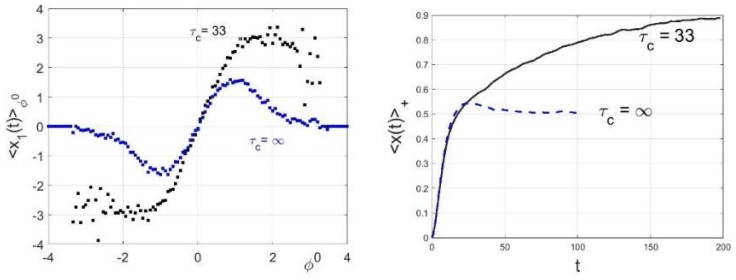

FIG. 13: Ordered perpendicular displacements $\langle x_1(t)\rangle_{\varphi^0}$ versus φ^0 (left) and $\langle x_1(t)\rangle_+$ as function of t (right) for a time-dependent potential with $\tau_c = 33$ compared to the static case $\tau_c = \infty$.

Significant differences appear for both directions. One can see in Fig. (15, left panel) that the perpendicular displacements $\langle x_1(t)\rangle_{\varphi^0}$ are larger in time-depending potential, although the calculations are at a very large time, $t = 6\tau_c$ (where the EC of the potential (3) is negligible, $E(t) = 10^{-8}$). The main contribution comes from large values of the potential $|\varphi^0|$, which is negligible in the static potential. The amplitude of the ordered motion is defined by the displacements conditioned by the sign of φ^0, $\langle x_1(t)\rangle_+$ obtained by integration over φ^0 on the interval $[0, \infty)$. The time derivatives of these functions determine the hidden drifts [2-4], a pair of average velocities with opposite directions that exactly compensate each

other. Surprisingly, the time evolution of $\langle x_1(t)\rangle_+$ shows a continuous increase in time-dependent potential, while it saturates in the static case, as seen in Fig. (15, right panel). This means that the hidden drifts are transitory in static potentials, but they are long-life statistical quantities in time dependent potential. Their amplitude decays on a long time scale, much longer than the decorrelation time of the potential.

The time variation of the potential also modifies the parallel displacements $\langle x_2(t)\rangle_{\varphi^0}$ by determining the extention of the contribution on the whole range of φ^0 and the dependence of these quantities on φ^0. It is peaked on $\varphi^0 = 0$ and has a weak (algebraic) decay at lage $|\varphi^0|$, instead of the concentration on the domain of free trajectories with uniform average displacement Eq. (28). However, the average Lagrangian velocity is uniform on the whole range of φ^0 and it has the Eulerian value V_d. The process of concentration of the Lagrangian average velocity on the domain of free trajectories found in static potentials is eliminated by the time-variation.

- Trajectory distribution and transport

The fluctuations of the trajectories $\left\langle \delta x_i^2(t)\right\rangle_{\varphi^0}$ and the transport $\langle \delta x_i(t)\delta v_i(t)\rangle_{\varphi^0}$ conditioned by the initial potential are all asymptotically uniform on the whole domain of φ^0. They reach this stage in a long time compared to the correlation time of the potential ($t \gg \tau_c$) staring from the values corresponding to static potential that are maintained at small time $t < \tau_c$.

Trajectory dispersion has nonstandard time-dependence in both directions

$$\langle \delta x_1^2(t)\rangle \sim t^{0.57},\ \left\langle \delta x_2^2(t)\right\rangle \sim t^{1.35}, \tag{31}$$

which corresponds to subdiffusive perpendicular transport (but not saturated as in the static case) and superdiffusive parallel transport (but not of ballistic type).

- The cause of the anomalous Lagrangian statistics

The persistent Lagrangian order and the non-standard characteristics of the trajectories in the time dependent case can be understood by analysing the statistics of the Lagrangian potention $\varphi(t) \equiv \varphi(x(t), t)$. The distribution of the Lagrangian potential has the same invariance property as the Lagrangian velocity. It has the Gaussian probability of the Eulerian potential for both the static and the time-dependent case, at any value of the average velocity V_d. However, significant differences appear between these cases concerning the correlation and the average conditioned by the initial potential, as seen in Fig. (14).

The correlation of the Lagrangian potential $L_\varphi(t) = \langle \varphi(0)\ \varphi(t)\rangle$ is far from the Eulerian time-correlation, $E(0,t)$, except for the trivial case of static potential with $V_d = 0$, where the invariance of the potential implies $L_\varphi(t) = \ E(0,t) = 1$. In all the other cases shown in Fig. (14), the Lagrangian correlation is stronger than the Eulerian one, as it has a long tail with much slower decay. It demonstrates that the Lagrangian potential has a long-time memory.

The memory effect is strongest in static potentials with average velocity $V_d = 0$. The Lagrangian correlation decreases much slower than the Eulerian one, and it is larger than $E(0,t)$ at any time (Fig. (14), the curve for $V_d = 0,\ \tau_c = 33$) . In this example, at $t = 200 \cong 6\tau_c$, L_φ decreases only at 0.4, while $E(0,t) = 1.5\ 10^{-8}$.

The average velocity ($V_d \neq 0$) determines a faster decrease of $L_\varphi(t)$ at small time that leads to smaller values compared to the case $V_d = 0$ (Fig. (14), the curve for $V_d = 0.3,\ \tau_c = 33$) . The decorrelation takes place on two time-scales. There is a fast decay at small time that is followed by a slaw decrease of $L_\varphi(t)$. The fast decay at small t is the same for $\tau_c = \infty$ and $\tau_c = 33$, which shows that this process is not a consequence of the potential variation, but rather of the presence of V_d. In the static case, the momory of the Lagrangian potential is infinite ($L_\varphi(t)$ saturates).

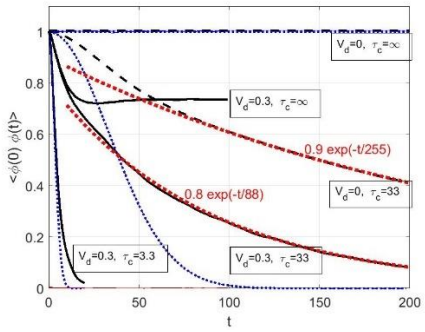

FIG. 14: Correlation of the Lagrangian potential for $V_d = 0$ (dashed) and $V_d = 0.3$ (continuous) for static ($\tau_c = \infty$), slow ($\tau_c = 33$) and fast time-variation ($\tau_c = 3.3$), compared to the Eulerian correlations (dotted blue). Exponential long tails with appear at large τ_c.

A selective decorrelation mechanism determined by the average velocity appears in static potentials and for weak time-variation (large τ_c) . This process can be understood by analysing the correlation of $\varphi(t)$ conditioned by the category $c = tr,\ fr$ in the static potential ($\tau_c = \infty$). $\langle \varphi(0)\ \varphi(t) \rangle_c$ decays to zero for the free trajectories, while it saturates for the trapped trajectories at a value that is comparable to φ^0. This demonstrates that in static potential the decorrelation affects only the free trajectories and that the memory effect is determined by the trapped trajectories, which approximately maintain the initial potential $\varphi(0)$.

The long memory of the potential and the increase and saturation of the average displacements $\langle x_1(t) \rangle_{\varphi^0}$ (Fig. 13) is the result of the same process. It consists of the liberation of the trapped trajectories with large $[\varphi^0]$ followed by repeated stochastic events of capture and release combined with the constraint of the total potential invariance (20) that approximately holds for small time intervals. The liberation of the trapped trajectories with large φ^0 is produced when the time variation determines the decrease of the potential to Δ. The contour lines of the potential that are open have the average perpendicular displacement $\frac{\Delta}{V_d}$ and the average potential along them equal to zero (as imposed by Eq. (20)). After a large number of capture/release events (which means at large time compared to τ_c), the stochastic recapture is uniformly distributed over the potential and has the average perpendicular location $\frac{\Delta}{V_d}$. This cancels asymptotically the average of the potentials of the trapping events and leads to the average $\frac{\Delta}{V_d}$ of the positions of the trapping events. This happens on a time scale that is much larger than τ_c. These released trajectories with large φ^0 determine the slow decay of their initial average potential and the increase of their average displacement from zero to the largest possible value. Thus, the memory of the Lagrangian potential and the strengthening of the coherence of the trajectories are both determined by the uniformization of the trapping events on the trajectories due to time-variation of the potential.

1.8 Conclusions

We have found that the statistical properties are completely different for the trapped (closed, periodic) trajectories compared to the free trajectories that reach large distances. Also, the existence of an average velocity V_d determines strong structural changes by generating coherence in the Lagrangian velocity.

For $V_d = 0$, all trajectories are trapped at large time. They form coherent structures of vortical type. The transport (the time dependent diffusion coefficient $D_i(t)$) is determined only by the trajectories that are free (still open at time t). It is subdiffusive due to the decay to zero of the fraction of this category.

The average velocity determines strong modifications of the Lagrangian statistics and important coherent effects. The fraction of free trajectories has a transitory decrease followed by saturation. They have Gaussian distribution with an average displacement along V_d. Trapped trajectories exist for small V_d . They have peaked distributions around the initial condition and form trajectory vortical structures. The Lagrangian velocity acquires coherent features for both categories. Average components of velocity are generated along V_d from the stochastic ones. The distributions of the Lagrangian velocity are invariant for both categories, but they are non-Gaussian. Thus, the statistical invariance of the Lagrangian velocity (Lumley theorem) is ensured in a rather non-trivial manner that involves a strong increase of the degree of coherence. Hidden coherent elements (average displacements or correlations conditioned by the initial potential φ^0) are identified. Their average over φ^0 is zero, which means that they do not determine average displacements or velocities, but they influence the dispersion of trajectories.

The transport is produced only by the free trajectories. A paradoxical behavior was found: the statistics of the trajectories is strongly non-Gaussian, but the transport is produced by Gaussian trajectories, which in fact yield from the non-Gaussian velocity distribution of the free trajectories.

We have shown that a slow time variation has not the expected effect of attenuation of the coherent component of the motion, but it determines long-time memory and increases the life of the hidden ordered elements.

[1] Vlad M, Spineanu F, Randon and quasi-coherent aspects in particle motion and their effects on transport and turbulence evolution, New Journal of Physics 19 (2017) 025014

[2] M. Vlad, F. Spineanu, Hidden drifts in turbulence, Europhysics Letters (EPL) 124, 60002 (2018).

[3] M. Vlad, F. Spineanu, Combined effects of hidden and polarization drifts on impurity transport in tokamak plasmas, Phys. Plasmas 25, 092304 (2018).

[4] M. Vlad, D.I. Palade, F. Spineanu, Effects of the parallel acceleration on heavy impurity transport in turbulent tokamak plasmas, 2021 Plasma Phys. Control. Fusion 63, 035007

[5] D. I. Palade and M. Vlad, Fast generation of Gaussian random fields for direct numerical simulations of stochastic transport, 2021 Statistics and Computing 31, 60

[6] D. I. Palade, M. Vlad, F. Spineanu, Turbulent transport of the W impurity ions in tokamak plasmas: properties derived from a test particle approach, 2021 Nuclear Fusion 61, 116031

[7] M. Vlad, D.I. Palade, F. Spineanu, Lagrangian coherent effects in the statistics of Hamiltonian motions, in preparation

2. Numerical simulations of intermittency effects on turbulent transport in the SOL and edge plasma.

2.1 Non-Gaussian features of intermittency in SOL

The developement of viable thermonuclear fusion reactors requires a good controll over the transport phenomena within the fusion plasmas. Unfortunately, it is known for several decades, that a confined hot plasma is plagued with a consistent level of turbulence. The later is directly responsible for undesirable heat and particle transport, especially across the radial direction, i.e. towards the center or the walls of the reactor. The nature of this type of motion can be either convective or diffusive. Such radial fluxes are dangereous, especially in the Scrape-Off-Layer (SOL) which absorbs most of the plasma exhaust and transfers it to the divertor. In this region, the turbulence amplitude is large compared to the plasma thermal energy. Therefore, understanding the turbulent transport in SOL is of outmost importance. The problem has been extensively studied in the past decades, but the involved phenomena are still not fully understood, in part due to the non-linear nature of the processes.

One particular aspect that is neglected in many studies of turbulent tranport is the presence of intermittency. The latter is represented by quasi-periodic, quasi-coherent, structures of fields and plasmas that exhibit high gradient, especially in the SOL. The most well known structures responsible for intermittency are Blobs, Alfven modes or Edge Localized Modes (ELMs). From a qualitative perspective, the intermittent features of turbulence are reflected in the distribution of field ϕ (or field gradients) values which depart from Gaussianity. While this departure is, in many instances, small compared with the gross PDF of field-values $P(\phi)$, it raises the question wether they are important or not for the transport.

In this report, we investigate the issue of how non-Gaussian turbulent stochastic fields affect the transport in biased incompressible 2D flows. This setup is a simplified model for the dynamics of charged particles in the SOL region in a tokamak plasma.

2.2 Theory

We consider that, in the SOL region of a tokamak plasma, the magnetic field B is strong, constant, and oriented in the parallel direction along the Oz axis, $B = B_0\hat{e}_z$. Thus, we assume the slab-geometric limit. Charged particles move mainly due to the **ExB** drift induced by the presence of a turbulent field $\phi(\boldsymbol{x}, t)$, $\boldsymbol{x} = (x, y)$ and due to an effective poloidal drift V_p. The latter is oriented in the Oy direction and tries to mimic the poloidal flow and the neoclassical contributions to drifts. Thus, in this slab-geometrical setup, the trajectories of particles are described by the guiding-center equation of motion:

$$\frac{d\boldsymbol{x}(t)}{dt} = V_p\hat{e}_y + \hat{e}_z \times \nabla\phi$$

A statistical approach to the posed problem is to consider an ensemble of stochastic trajectories $\{\boldsymbol{x}(t)\}$ driven via the equation of motion by a stochastic ensemble of random field $\{\phi(\boldsymbol{x},t)\}$. The latter must reproduce the desired Eulerian statistical properties of turbulence, field distribution $P(\phi)$ and correlation $E(\boldsymbol{x},t) = F_{\boldsymbol{x},\boldsymbol{t}}(S(k,\omega))$, with the spectrum $S(k,\omega) =< \left|\tilde{\phi}(k)\right|^2 >$. The transport coefficients can be easily evaluated as statistical averages over the ensemble of trajdctories $2D(t) = d_t\langle x^2(t)\rangle = 2\langle v(0)x(t)\rangle$.

While this type of transport is widely non-linear, some results are known. We can use the characteristic correlation length λ_c, the correlation time τ_c and the field amplitude $V = \Phi/\lambda_c$ with $\Phi = \sqrt{\langle\phi^2(0)\rangle}$ to define the Kubo number:

$$K_\star = \frac{\tau_c}{\tau_{fl}} = \frac{\Phi\tau_c}{\lambda_c^2}$$

The time of flight is defined as $\tau_{fl} = \lambda_c/V$; The Kubo number is a measure of the turbulence strength. One can identify two limiting cases:

- The quasi-linear regime (weak turbulence/high-frequency $K_\star \ll 1$. The diffusion coefficients can be shown to have the following dependency $D^\infty \sim K_\star^2\lambda_c^2/\tau_c$
- The strong limit (strong turbulence/ low frequency $K_\star \gg 1$. The diffusion is anomalous, and it has been shown to decay as $D^\infty \sim K_\star^{1-\gamma}, \gamma = 0.3$

In order to investigate the turbulent transport in the present, test-particle, approach, one needs statistical informations on the turbulent fields. In particular, we need to know the distribution of field values $P(\phi)$ and the power spectrum $S(k,\omega) =< \left|\tilde{\phi}(k)\right|^2 >$. Such information is, in general, scarcely available from experimental diagnostics. Most measurements are performed at the edge of the plasma, the core being mostly off-limits for the time being for diagnostic techniques. The results are also supported by gyrokinetic simulations and show that, as expected, the PDF of electrostatic turbulence is mostly Gaussian with some small deviations. Experimental evidence Riva et al. (2019); van Milligen et al. (2005); Gon¸calves et al. (2018); Beadle & Ricci (2020); Wang et al. (2019) indicates that, in the edge and SOL regions, the potential is approximately Gaussian $P(\phi) \sim \exp(-\phi^2)$ at negative values $\phi < 0$ and has an exponential-like distribution $P(\phi) \sim \exp(-\lambda|\phi|)$ in the positive range $\phi > 0$. This is equivalent with a change both of the skewness and kurtosis of the distribution. Note that the departure from Gaussianity is rather the rule than the exception: all turbulence models (Navier-Stokes, Hasegawa- Mima, Vlasov-Maxwell, etc.) include convective non-linearities which lead, implicitly, to non-Gaussian solutions Anderson & Botha (2015); Anderson & Hnat (2017).

Regarding the spectrum, it is well known that the dynamics of ions is dominated by low-frequency microturbulence (ITG, TEM) which, in most regimes, has some coherent qualitative features: a fast decay in frequency and along the radial direction with a peaked profile (at some specific wave-number k_0) along

the poloidal direction Shafer et al. (2012); Fonck et al. (1993); Holland et al. (2009); Jenko & Dorland (2002); Casati et al. (2009); Qi et al. (2019).

Thus, we are interested in generating numerically at some point slighlty non-Gaussian random fields with known Eulerian correlation (or, equivalently, spectrum). This turns out to be a difficult problem. While there are plenly of techniques to generate random normal fields, the problem of departure from Gaussianity is somehow more involved. For this reason, we assume the following mapping: a non-Gaussian random field ϕ can be constructed from an auxiliary Gaussian random field φ through a non-linear local transformation f, such that $\phi(\boldsymbol{x},t) = f\big(\varphi(\boldsymbol{x},t)\big)$. The function must be chosen such that the first two-moments are preserved $\langle\phi(\boldsymbol{x},t)\rangle = \langle\varphi(\boldsymbol{x},t)\rangle = 0$ and $\langle\phi(\boldsymbol{x},t)\phi(\boldsymbol{x}',t')\rangle \approx \langle\varphi(\boldsymbol{x},t)\varphi(\boldsymbol{x}',t')\rangle = E(\boldsymbol{x}-\boldsymbol{x}',t-t')$.

It this framework it can be easily shown that the homogeneity of $\varphi(x)$ is easily transfered to $\phi(x)$ and the correlation of field derivatives obeys:

$$\langle\partial_i\phi(\boldsymbol{x},t)\partial_j\phi(\boldsymbol{x}',t')\rangle = \langle f'[\varphi(\boldsymbol{x},t)]f'[\varphi(\boldsymbol{x}',t')]\partial_i\varphi(\boldsymbol{x},t)\partial_j\varphi(\boldsymbol{x}',t')\rangle$$

Also, the skewness and excess of kurtosis can be computed as :

$$s = \frac{\langle\phi^3(\boldsymbol{x},t)\rangle}{\langle\phi^2(\boldsymbol{x},t)\rangle^{\frac{3}{2}}} = \frac{\langle f[\varphi]^3\rangle}{\langle f[\varphi]^2\rangle^{\frac{3}{2}}}$$

$$\delta\kappa = \frac{\langle\phi^4(\boldsymbol{x},t)\rangle}{\langle\phi^2(\boldsymbol{x},t)\rangle^2} - 3 = \frac{\langle f[\varphi]^4\rangle}{\langle f[\varphi]^2\rangle^2} - 3$$

Since the experimental evidence for SOL turbulence indicates small deviations from Gaussianity, we choose a simple non-linear transformation $f(\varphi) \sim \varphi + \alpha\,\varphi^2 + \beta\,\varphi^3 - \alpha\,V_0$. With this, the following particular results are valid:

$$\phi = \frac{\varphi + \alpha\varphi^2 + \beta\varphi^3 - \alpha V_0}{\sqrt{1 + 2\alpha^2 V_0 + 3\beta V_0(2 + 5\,\beta V_0)}}$$

$$\partial_i\phi = \frac{1 + 2\alpha\varphi + 3\beta\varphi^2}{\sqrt{1 + 2\alpha^2 V_0 + 3\beta V_0(2 + 5\,\beta V_0)}}\partial_i\varphi$$

$$s \approx 6\alpha V_0^{\frac{1}{2}}(1 + 3\beta V_0)$$

$$\delta\kappa \approx 24\beta V_0 + 144\beta^2 V_0^2 + 48\alpha^2 V_0$$

$$E' = E\,\frac{2\alpha^2 E + 6\beta^2 E^2 + (1 + 3\beta V_0)^2}{1 + 2\alpha^2 V_0 + 3\beta V_0(2 + 5\,\beta V_0)}$$

Note that, up to first order, the skewness is controlled by the parameter α while the kurtosis by β. Supplementary, the correlation is virtually unchanged due to its second order parametric dependence $E' \approx E + 2\alpha^2 E(E - V_0) + 6\beta^2 E(E^2 - V_0^2)$. This enables us to approximate $E' \approx E$ since $\alpha, \beta \sim 10^{-1}$ for a good agreement with experimental distributions [36, 48].

2.3 The Decorrelation Trajectory Method (DTM)

The Decorrelation Trajectory Method (DTM) is a semi-analytical method that aims at computing the diffusion coefficients driven by stochastic random fields, i.e. turbulence. It has been used previously to investigate the turbulent transport in tokamak plasmas Vlad et al. (1998a); Croitoru et al. (2017); Vlad et al. (2004); Vlad & Spineanu (2016) as well as in some astrophysical systems Negrea (2019). The method relies on a set of deterministic objects called Decorrelation Trajectories (DT's) Vlad et al. (1998a) which are used to compute the diffusion 2.12:

$$\frac{d\boldsymbol{X}^S(t)}{dt} = \boldsymbol{V}^S(\boldsymbol{X}^S(t), t)) = \widehat{e_z} \times \Phi^S(\boldsymbol{X}^S(t), t) + \boldsymbol{V}_p$$
$$D_{xx}(t) = \langle v_x(0)x(t)\rangle \approx \int dS\, P(S) V_x^S(\mathbf{0}, 0) X^S(t)$$

The method is, essentially, an approximation which assumes that trajectories that have similar initial conditions remain very similar at larger times. If this is true, one can replace the ensemble of real stochastic potentials $\phi(\boldsymbol{x}, t)$ with a set of deterministic conditional potentials $\Phi^S(\boldsymbol{x}, t)$which are defined as conditional averages over real potentials in subsensembles (S), i.e. $\Phi^S(\boldsymbol{x}, t) = \langle \phi(\boldsymbol{x}, t)\rangle^S$.

In our case, when the field is non-Gaussian, the subsensembles are defined as it follows:

$$S = \left\{\phi(\boldsymbol{x}, t) = f\big(\varphi(\boldsymbol{x}, t)\big) \,\middle|\, \partial_i \varphi(\mathbf{0}, 0) = \varphi_i^S \,; i \in \{0, x, y\}\right\}$$
$$P(S) = \prod_i e^{-\frac{\left(\varphi_i^S\right)^2}{2V_{ii}}} \quad ; \quad V_{ii} = \langle |\partial_i \varphi(0,0)|^2\rangle = -\partial_{ii} E(0,0)$$
$$\Phi^S(\boldsymbol{x}, t) = \langle f[\varphi(\boldsymbol{x}, t)]\rangle^S = \frac{\Psi^S(\boldsymbol{x}, t)(1 + 3\beta\sigma) + \alpha(-1 + \sigma + \Psi^S(\boldsymbol{x}, t)^2) + \beta\Psi^S(\boldsymbol{x}, t)^3}{\sqrt{1 + 2\alpha^2 + 6\beta + 15\beta^2}}$$

$$\Psi^S(\boldsymbol{x},t)=\sum_i \varphi_i^S \frac{\partial_i E(\boldsymbol{x},t)}{V_{ii}}$$

$$\sigma = V_0 - \sum_i \frac{\left(\partial_i E(\boldsymbol{x},t)\right)^2}{V_{ii}}$$

The function σ is a measure of the field fluctuations within a subensemble S and it turns out to be precisely $\sigma = \langle|\varphi(x,t)-\langle\varphi(x,t)\rangle^S|^2\rangle^S = \langle|\varphi(x,t)|^2\rangle^S - |\langle\varphi(x,t)\rangle^S|^2$.

2.4 Direct numerical simulations

The method of direct numerical simulations (DNS) aims at describing the turbulent transport without resorting to any approximation. The main idea is to generate a statistical ensemble of numerical random fields $\{\phi(x,t)\}$ with appropriate statistical properties and investigate the transport of particles $\{x(t)\}$ within this ensemble. The diffusion coefficient can be computed as Lagrangian average over these trajectories $2D(t) = d_t < x^2(t) >$. In some sense, DNS tries to reproduce numerically, the reality of turbulent motion.

In order to achieve this goal, we follow the same recipe described above. We generate the Gaussian Random fields $\varphi(\boldsymbol{x},t)$ as:

$$\varphi(\boldsymbol{x},t)=\sqrt{\frac{2}{N_c}}\sum_{j=1}^{N_c}\sin\left(\boldsymbol{k}_j\boldsymbol{x}-\omega_j t+\alpha_j\right)$$

Where $\boldsymbol{k}_j$ are random vectors generated from a PDF which is equal with the spectrum $S(k)$. The same is true for random frequencies ω_j and the random phases $\alpha_j \in (0,2\pi)$. Note that all these random variables used to construct the random fields are independent one from another. In practice, we used $N_c \sim 10^3$ in most simulations and an ensemble of dimension $N_p \sim 10^6$. Having these GRFs at hand, it is almost straightforward to solve the problem of interest for non-GRFs ϕ using the explicit form for the equation of motion:

$$\frac{d\boldsymbol{x}(t)}{dt} = f'[\varphi(\boldsymbol{x}(t),t)]\hat{e}_z \times \nabla\varphi(\boldsymbol{x}(t),t) + \boldsymbol{V}_p$$

2.5 Analytical estimations

Before diving into numerical results obtained with the above described theoretical methods (DTM and DNS) it is important to get a simplified glimpse of what to expect from the effects of non-Gaussianity on the turbulent transport. We attempt an analytical treatment.

In all investigations we shall use two simple models of turbulence spectrum/correlation, described by :

$$E_1(x,y,t) = e^{-\frac{x^2}{2\lambda_x^2}-\frac{y^2}{2\lambda_y^2}-\frac{t}{\tau_c}}$$

$$E_2(x,y,t) = \left(1+\frac{x^2}{\lambda_x^2}+\frac{y^2}{\lambda_y^2}\right)^{-1} e^{-\frac{t}{\tau_c}}$$

With $\lambda_x = \lambda_y = 1, \tau_c = 10$, thus $V_0 = 1$. These choices are in agreement with gross properties of turbulence spectra from incompressible plasma and fluids. We show in Fig. 1 how the proposed transformation $f(\varphi) \sim \varphi + \alpha\varphi^2 + \beta\varphi^3 - \alpha$ distorts the Gaussian distribution both for the potential and its derivatives. Note how, through appropriate combinations of α and β (the brown line), the resulting PDF is closer to Gaussianity on the negative domain $\varphi < 0$ and similar to an exponential distribution in the positive part $\varphi > 0$ (as observed in measurements). Also, due to the relation between ∂iϕ and ϕ, the distribution of derivatives $P(\partial_i\varphi)$ is free of any skewness. In Figs. 2a,2b we plot the change in correlation $\delta E = E' - E$ under the effects of non-Gaussianity for the first model, E1. The results are in agreement with the analytical estimation 2.6 that the departure is $\delta E \sim O(\alpha^2, \beta^2) \sim 1\% E$ and virtually negligible, especially in the strong correlated area |x| ∼ 0. For E_2 the profiles are extremely similar.

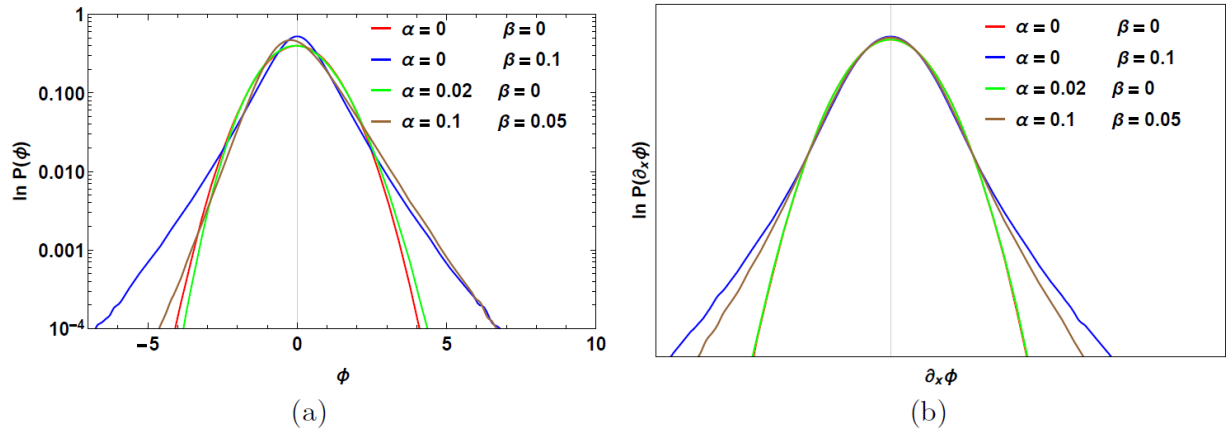

Figure 1: PDF of potential values (left) and potential derivatives (right) generated randomly in accordance with the non-linear transformation from eqn. of motion.

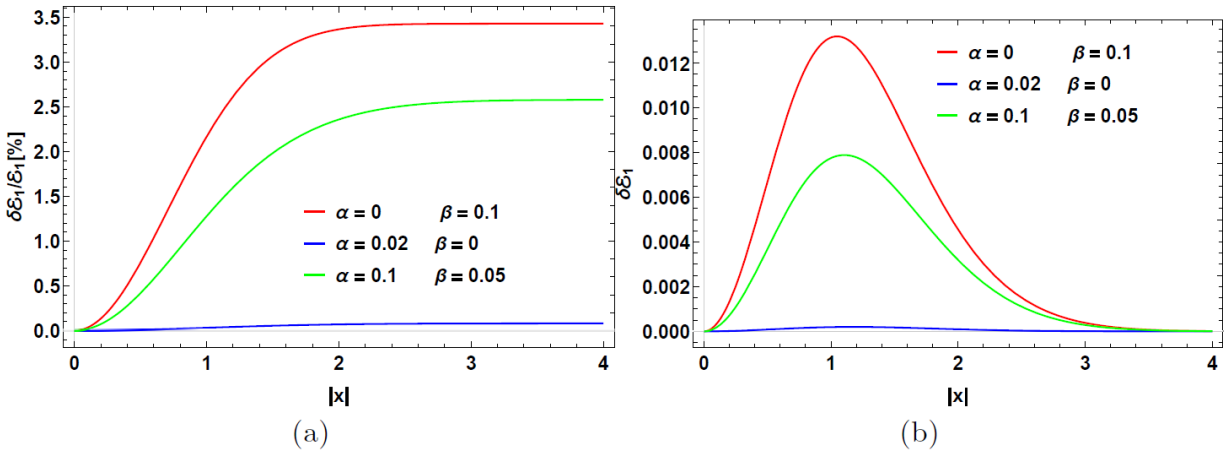

(a) (b)

Figure 2: Relative changes $\delta E = E_1' - E_1$ of the correlation function on the spatial domain at different small α, β values.

We start by considering the simplified case of frozen turbulence, when the turbulent potential has virtually no time dependence $\varphi(x,t) \equiv \varphi(x)$. This case can be obtained from the perspective of the correlation function setting $\tau_c \to \infty$. The equations of motion have a Hamiltonian nature, thus the trajectories are closed and conserve the potential values $\varphi(\boldsymbol{x}(t),t) = \varphi(\boldsymbol{x}(0),t) = \varphi(\boldsymbol{0}) \to \phi(\boldsymbol{x}(t),t) = \phi(0)$. We also define:

$$A = \frac{1 + 2\alpha\varphi + 3\beta\varphi^2}{\sqrt{1 + 2\alpha^2 + 3\beta(2 + 5\beta)}}$$

Using this notation, one can relate the trajectories in the Gaussian case (0) with the ones from the non-Gaussian case, using the equations of motion:

$$\frac{d\boldsymbol{x_0}(t)}{dt} = \hat{e}_z \times \nabla\varphi(\boldsymbol{x_0}(t))$$

$$\frac{d\boldsymbol{x}(t)}{dt} = A[\varphi(0)]\hat{e}_z \times \nabla\varphi(\boldsymbol{x}(t))$$

We can perform a variable transformation $x(t) = x_0(A[\varphi]t)$ and compute the diffusion coefficients in both cases (Gaussian and non-Gaussian):

$$D(t) = \int d\varphi(0) P[\varphi(0)] d_0\big(A[\varphi(0)]t; \varphi(0)\big) A[\varphi(0)]$$

$$D_0(t) = \int d\varphi(0) P[\varphi(0)] d_0\big(t; \varphi(0)\big)$$

$$d_0\big(t;\varphi(0)\big) = \frac{d}{2dt}\langle x_0^2(t)\rangle_{\varphi(0)}$$

By the virtue of a generalized mean theorem, we can obtain:

$$D(t) = A\big[\varphi_{eff}(t)\big]D_0[A[\varphi_{eff}(t)t]$$

Supplementary, the diffusion in our case of interest is known to be anomalous, $D(t) \sim t^{-\gamma}, \varphi_{eff}(t) \sim t^{-\zeta}$. Approximating the asymptotic values with saturation at the decorrelation time τ_c we obtain th following analytical approximations :

$$\begin{cases} \dfrac{D^{\infty}}{D_0^{\infty}} = A\big[\varphi_{eff}(\tau_c;\alpha,\beta)\big]^2 \approx 1 + 2\alpha^2 + 12\beta^2, & K_\star \ll 1 \\ \dfrac{D^{\infty}}{D_0^{\infty}} = A\big[\varphi_{eff}(\tau_c;\alpha,\beta)\big]^{1-\gamma} \approx 1 + 3\beta(-1+\gamma), & K_\star \gg 1 \end{cases}$$

Thus, we conclude at this end that the effect of non-gausianity is only quadratic in the quasi-linear regime, while in the strong turbulence case is roughly linear in β , thus in kurtosis. The skewness has a much lower effect. In order to quantify such behavior we define a susceptibility function

$$\chi = \lim_{\delta\kappa\to 0}\frac{1}{\delta\kappa}\left(1 - \frac{D^{\infty}(\delta\kappa)}{D^{\infty}(0)}\right)$$

2.6 Numerical results

We move now further to the numerical realm. Our intention is to test if the analytical estimations have real meaning in full non-linear regimes. For that, the statistical methods that were described above (DNS and DTM) will be used. The DNS method is, in principle, exact but requires consistent CPU resources. In contrast, the DTM method relies heavily on a smart approximation leading to not-so-accurate results but at a low CPU cost. The purpose of DTM is to serve as a supplementary test for DNS.

Before looking specifically to the effect of non-Gaussianity is important to review the quantitative features of diffusion transport coefficient from the Gaussian case. For that, we choose $\alpha = \beta = 0$, set $\tau_c = 10$ or $\tau_c \to \infty$ and $\lambda_x = \lambda_y = 1$. One can see in Fig 3 how the diffusion $D(t)$ grows up to a maximal value around the time of flight τ_{fl}, than decays algebraically towards 0 at larger times in the case of frozen turbulence $\tau_c \to \infty$. The presence of a finite decorrelation time $\tau_c = 10$ leads to a saturation process for the running diffusion coefficient. We note that DTM is able to reproduce qualitatively the DNS results but tends to

overestimate the decay of diffusion. This happens since DTM overestimated by design the trapping processes.

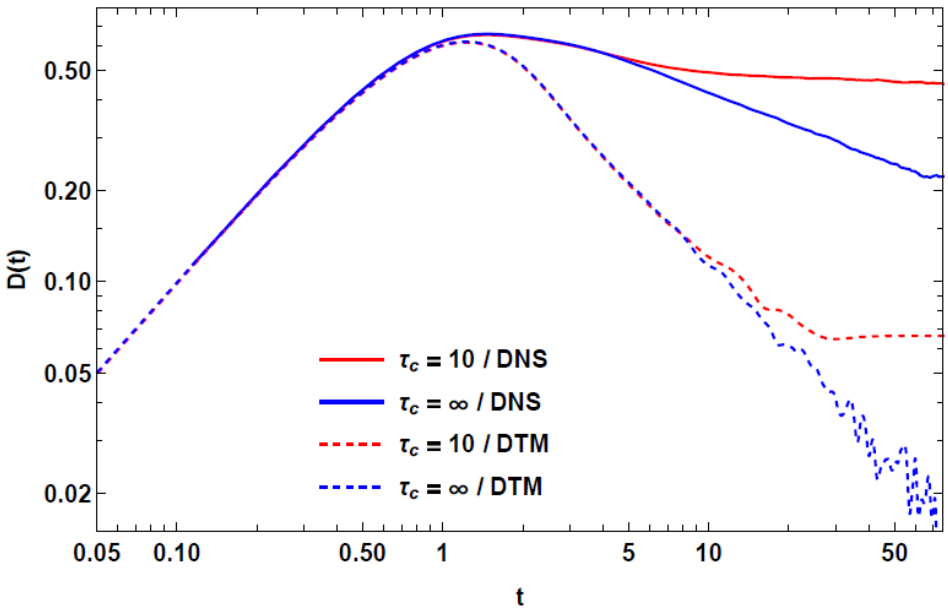

Figure 3: Running diffusion coefficient D(t) obtained for the correlation E1, Vp = 0 in the case τc → ∞ (blue) and τc = 10 (red) with the use of DNS (full line) and DTM (dashed line).

Moving further to the non-Gaussian case, we set $\beta = 0, \tau_c = 10, V_p = 0$ and run multiple numerical simulations using both DTM and DNS. The results for the asymptotic diffusion D^{∞} are shown in Fig. 4. It turns out that both methods predict an asymetric variation of D^{∞} with the skewness s. But, the variations are so small $\sim 0.1\%$ that they can be safely neglected. Thus, the analytical result that the diffusion is not affected by skewness is validated by numerical data.

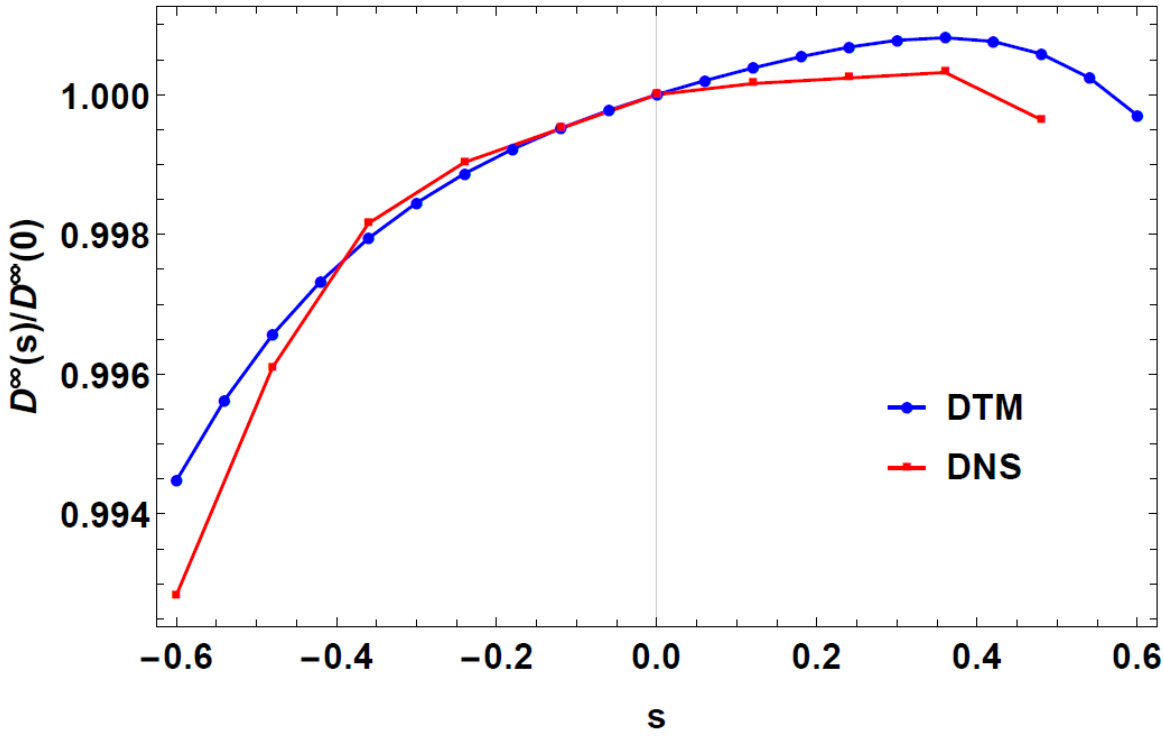

Figure 4: Asymptotic values of diffusion at β = 0, τc = 10, Vp = 0 vs. the skewness sobtained with the use of DTM (blue line) and DNS (red line).

Now we turn out attention towards the influence of β parameter. We set $\alpha = 0$ and perform multiple simulations. In Fig. 5 one can see the running diffusion profiles $D(t)$ obtained at different β values. Clearly, a strong effect is present. Regarding the values of the asymptotic diffusion D^{∞}, we show their variation with β in Fig. 6

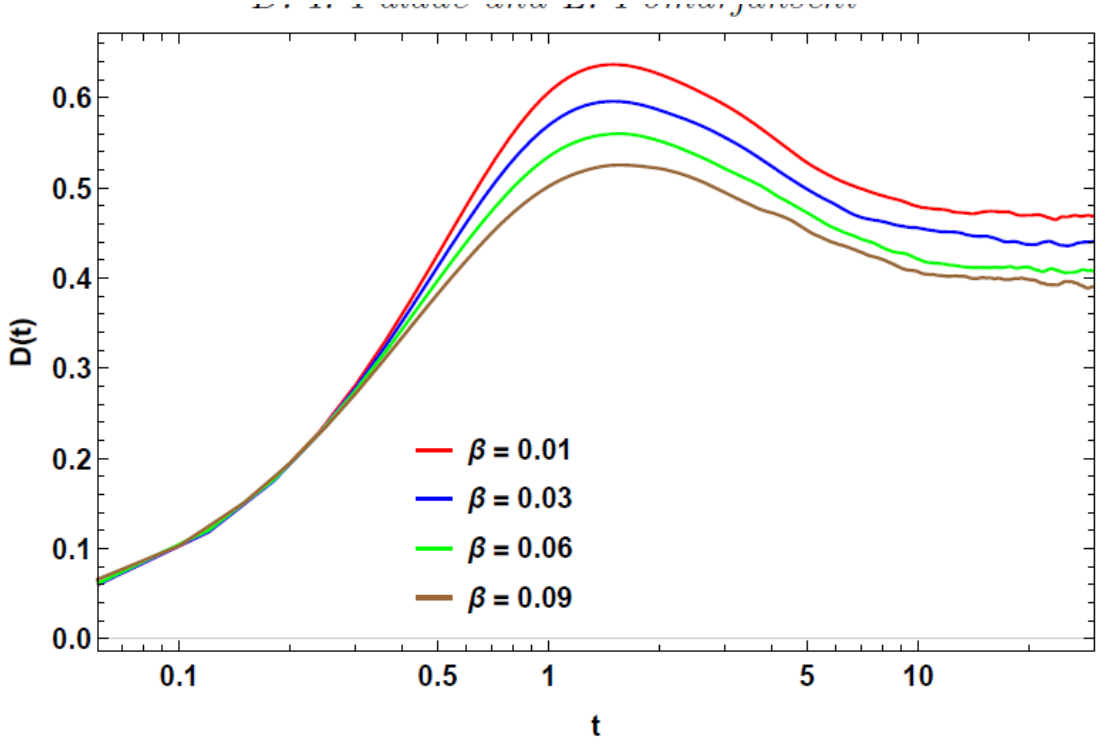

Figure 5: Running diffusion profiles D(t) obtained with DNS for the correlation E1 with τc = 10 and Vp = 0 at different β values and α = 0.

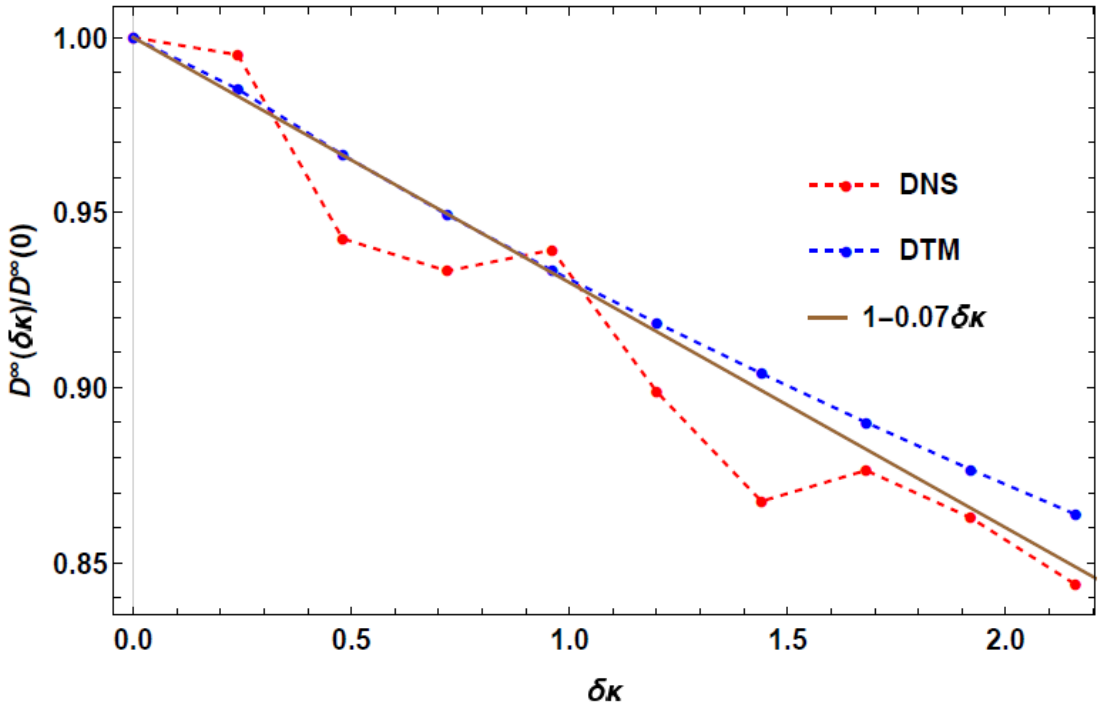

Figure 6: The relative asymptotic diffusion dependence with the excess kurtosis obtained with DTM for E2 (blue line) and with DNS for E1 (red line).

We plot in Fig. 6 asymptotic diffusion coefficients computed for different values of excess kurtosis. The expectation that the dependency is linear is met by the numerical results. It is interesting to note how the DTM results are quite close to the DNS ones, despite the fact that DTM gives, in general, poor quantitative agreement.

At this point, we want to see if the well-known results of anomalous scaling for the 2D incompressible diffusion holds in the non-Gaussian case. For that, we run extensive simulations and plot if Fig. 7 de dependency of the asymptotic diffusion $D^{\infty}(K_{\star})$ at different β. The results are obtained with DNS. It turns out that the anomalous slope $\gamma \approx -0.3$ is quite robust against non-Gaussianity and validates the Ischenko's result to general distributions.

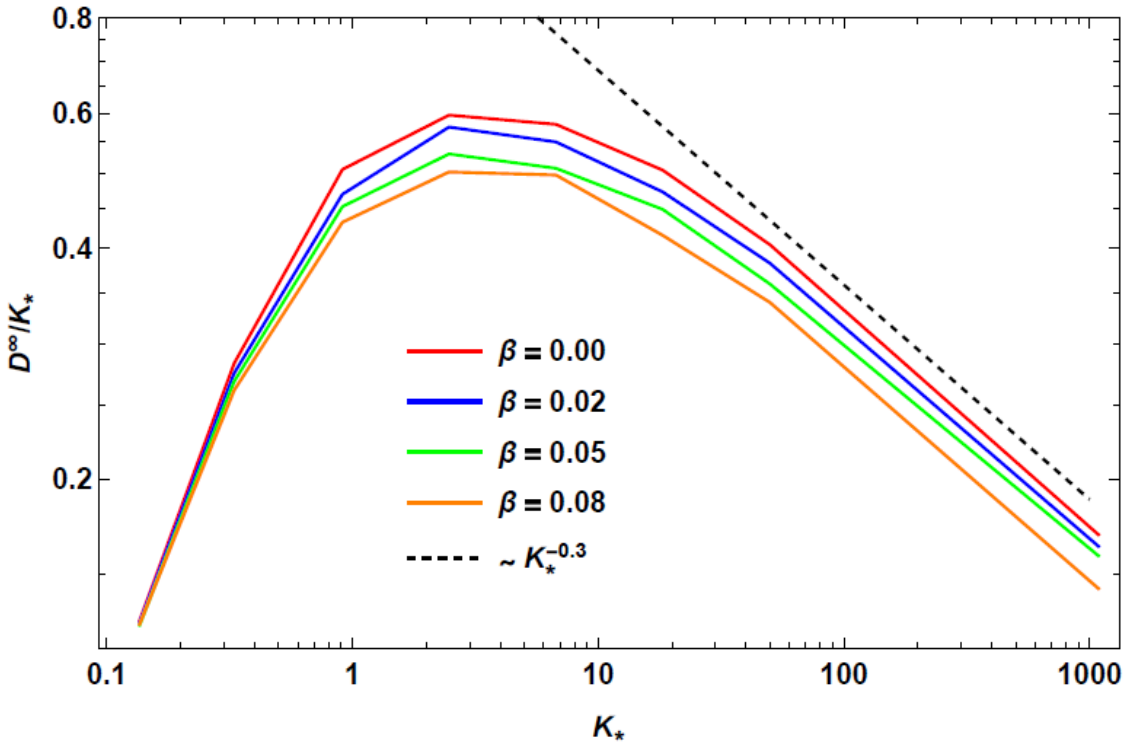

Figure 7: Asymptotic diffusion coefficient vs. the Kubo number at different β values. The results are obtained with DNS for E1 and Vp = 0.

Finally, let us try and characterize the relation between the linear susceptibility χ and the Kubo number $K_{\star}$. We plot in Fig. 8, this dependency at different V_p values.

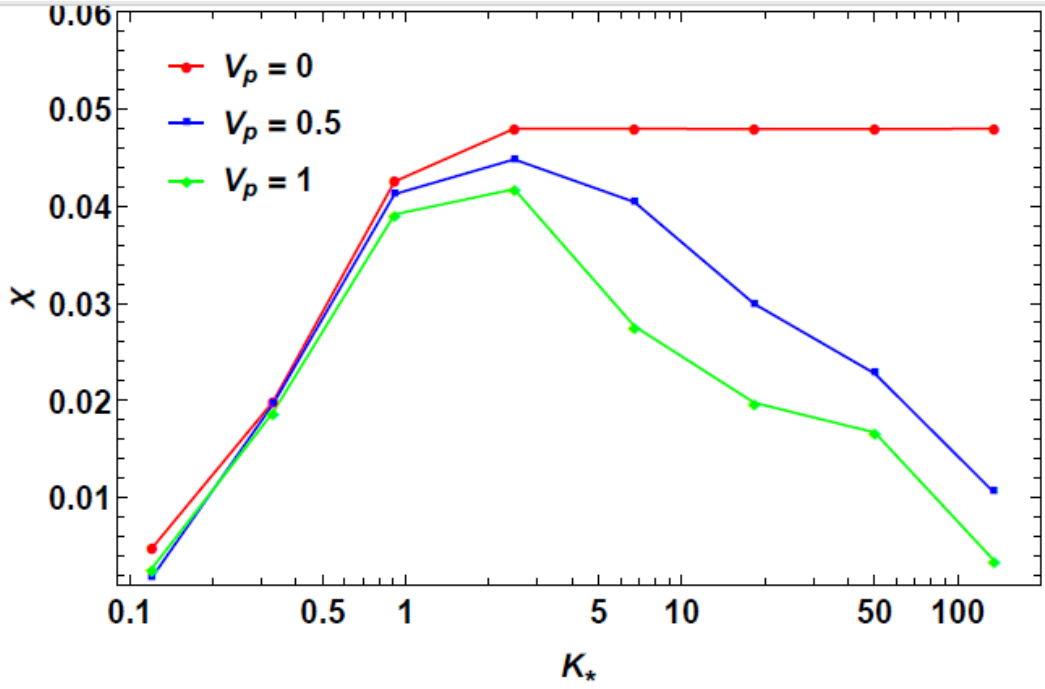

Figure 8. Susceptibility χ as a function of Kubo number K⋆ obtained with DNS for E1 at distinct Vp values.

2.7 Discussions and conclusions

We have used two different theoretical, statistical, approaches to investigate the turbulent transport of charged particles in turbulent media characterized by non-Gaussian features. This setup is relevant for the transport within fusion plasmas in the SOL region where non-Gaussian features are proeminent due to intermittent phenomena.

A semi-analytical analysis suggested that the departure from normal behavior through non-zero skewness and kurtosis leads to a linear decrease of diffusion with the excess of kurtosis. Complementary, the skewness can be neglected. This behavior is confirmed by the numerical analysis that employed the Decorrelation Trajectory Method and the Direct Numerical Simulation approach.

Moreover, we quantify this behavior using a response function like quantity χ which turns out to be dependent on the regime of turbulence, in particular the Kubo number $\chi(K_\star)$. In the quasilinear regime, the effects of intermittency are small $\chi \to 0$. At the other end of the spectrum, $K_\star \gg 1$, χ saturates to a maxima which is reached after the time of flight τ_{fl}, i.e. $K_\star \sim 1 - 2$. The presence of a poloidal velocity induces an algebraic decay of the susceptibility $\chi(K_\star) \sim K_\star^{-\gamma}$ in the non-linear regime. We summarize our findings trough the following relations

$$\begin{cases} D^{\infty}(\delta\kappa, s) \approx D^{\infty}(0,0)(1+\chi(K_{\star})\delta\kappa) \\ \chi(K_{\star}) \propto K_{\star}^{2}, \quad K_{\star} \ll 1 \\ \chi(K_{\star}) \sim K_{\star}^{-\gamma}, \quad K_{\star} \gg 1 \\ max\big(\chi(K_{\star})\big) \approx \chi\big(\tau_c = \tau_{fl}\big) \end{cases} .$$

Acknowledgement

This work has been carried out within the framework of the EUROfusion Consortium, funded by the European Union via the Euratom Research and Training Programme (Grant Agreement No 101052200 — EUROfusion). Views and opinions expressed are however those of the author(s) only and do not necessarily reflect those of the European Union or the European Commission. Neither the European Union nor the European Commission can be held responsible for them.

Conclusion

The effect of quasi-coherent components of the stochastic motion on the turbulent transport was investigated. A detailed Lagrangian study of trajectories in 2-dimensional incompressible velocity fields was employed to determine the statistical properties of the trapped (tr) and free (fr) particles. The origin of coherence was identified. Supplementary, it was shown that the time variation of the potential does not hinder the Lagrangian coherence and that it generates long time memory.

The turbulence in the SOL region of a tokamak plasma is, many times, plagued by intermittent phenomena. As a consequence, the distribution of potential values of turbulent fields departs from Gaussianity. We investigated how this departure affects the turbulent transport of charged particle. A simplified transport model that captures the ExB drift as well as poloidal contributions was used to describe the trajectories of particles. The turbulence was modelled with the aid of a statistical approach called Direct Numerical Simulation. As a checking procedure, the Decorrelation Trajectory method was also used in this investigation. It was shown that the most proeminent feature that affects the transport is the kurtosis of the distribution of fields. This parameter induces almost linear variations of the diffusion coefficients. The response function is characterized numerically in detail regarding its dependence on plasma parameters captured by the Kubo number.

Papers

[1] D. I. Palade, L. Pomarjanschi, Effects of intermittency via non-Gaussianity on turbulent transport in magnetized plasmas, Journal of Plasma Physics , Volume 88 , Issue 2 , April 2022 , 905880202, DOI: https://doi.org/10.1017/S0022377822000022

Conferences

[1] "On the Existence of Hidden Coherent Motion of Particles and the Effects on Transport in Turbulent Plasmas and Fluids", Madalina VLAD, Dragos Iustin PALADE, Florin SPINEANU, The International Conference on Lasers, Plasma, and Radiation – Science and Technology, Bucharest, Romania, between June 7-10, 2022. (poster)

[2] "Effects of Non-Gaussianity on Turbulent Transport in Magnetized Plasmas and Astrophysical Systems", Dragos Iustin PALADE, Ligia POMARJANSCHI, The International Conference on Lasers, Plasma, and Radiation – Science and Technology, Bucharest, Romania, between June 7-10, 2022. (poster)